energies

Article

Controlling Factors and Forming Types of Deep Shale Gas Enrichment in Sichuan Basin, China

Xuewen Shi [1], Wei Wu [1], Qiuzi Wu [1,*], Kesu Zhong [1], Zhenxue Jiang [2,3] and Huan Miao [2,3]

[1] Shale Gas Research Institute, Petro China Southwest Oil and Gasfield Company, Chengdu 610021, China
[2] State Key Laboratory of Oil and Gas Resources and Exploration, Beijing 102249, China
[3] Institute of Unconventional Oil and Gas Science and Technology, China University of Petroleum (Beijing), Beijing 102249, China
* Correspondence: wuqiuzi@petrochina.com.cn

Abstract: In order to find out the enrichment mechanism and forming type of deep shale gas, taking the Longmaxi Formation shale in the Desheng–Yunjin Syncline area of Sichuan Basin as an example, we determined the mineralogy, organic geochemistry, physical property analysis, gas and water content, and the influence of three factors, namely sedimentation, structural conditions, and hydrogeological conditions, on the enrichment of shale gas. The results show that Longmaxi Formation shale in Desheng–Yunjin Syncline area is a good hydrocarbon source rock that is in the over-mature stage and has the characteristics of high porosity, low permeability, and high-water saturation. The contents of clay and quartz are high, and the brittleness index is quite different. According to the mineral composition, nine types of lithofacies can be found. The development characteristics of Longmaxi Formation shale and the sealing property of the roof have no obvious influence on the enrichment of shale gas, but the tectonic activities and hydrodynamic conditions have obvious influence on the enrichment of shale gas. The main control factors for shale gas enrichment in different regions are different. According to the main control factors, the gas accumulation in the study area can be divided into three types: fault-controlled gas, anticline-controlled gas, and hydrodynamic-controlled gas. The fault-controlled gas type is distributed in the north of the Desheng syncline and the north of the Yunjin syncline, the anticline-controlled gas type is distributed in the south of the Desheng syncline and the south of the Yunjin syncline, and the hydrodynamic-controlled gas type is distributed in the middle of the Baozang syncline. This result is of great significance for deep shale gas exploration.

Keywords: Sichuan basin; deep shale gas; Longmaxi Formation; shale gas enrichment mechanism; forming type

Citation: Shi, X.; Wu, W.; Wu, Q.; Zhong, K.; Jiang, Z.; Miao, H. Controlling Factors and Forming Types of Deep Shale Gas Enrichment in Sichuan Basin, China. *Energies* **2022**, *15*, 7023. https://doi.org/10.3390/en15197023

Academic Editor: Reza Rezaee

Received: 24 August 2022
Accepted: 22 September 2022
Published: 24 September 2022

1. Introduction

With the development of society and the surge of human demand for energy, shallow oil and gas resources can hardly meet China's energy demand [1,2]. As an important alternative field of oil and gas exploration and development in China, shale gas resources are of great significance to solving the energy demand by realizing the large-scale industrial development of shale gas [3–5].

The exploration and development of shale gas are always guided by the enrichment theory of shale gas. A lot of work has been done on the enrichment mode and influencing factors of shale gas in the past. Jiang et al. [6] believed that hydrocarbon generation evolutionary history and multiple tectonic activities were the main factors leading to differential enrichment of shale gas. Wang et al. [7] believed that the ancient sedimentary environment further affected the enrichment of shale gas by controlling the distribution characteristics of organic-rich shale; Hao et al. [8] believed that high TOC, high Ro, and later closed systems are the main reasons for shale gas enrichment. Yasin et al. [9] believed that

the sealing properties of the roof and floor are the key to shale gas enrichment in complex structural areas. Shi et al. [10] believed that the development characteristics of main faults have obvious control over the enrichment of surrounding shale gas, and they proposed three favorable enrichment structural styles. In conclusion, high organic matter abundance and high organic matter maturity are the basis for the large-scale generation of shale gas. Shale with a developed pore fracture system is a favorable reservoir for shale gas storage. A simple geological structure background and roof and floor with good sealing properties are the keys to shale gas preservation. In addition, water saturation is one of the important factors affecting shale gas enrichment. The higher the water content, the smaller the gas content [11–17]. However, these understandings are all derived from medium-shallow shale gas, and there have been few studies on the enrichment of deep shale at present.

As the main battlefield of deep shale gas exploration and development in China, many deep shale gas wells in Sichuan Basin and its periphery have obtained high-yield industrial gas flow [5,11,12,18]. Many years of exploration and development have shown that deep shale gas has the following problems compared to shallow shale gas: (1) the storage mechanism of deep shale gas is obviously different from that of shallow shale gas, and its storage state is unknown; (2) the preservation conditions of deep shale gas are complex, and the evaluation system is still in the exploration stage; (3) the gas production of a single well is high, the gas production of wells in the production area is general, and the enrichment mechanism of deep shale gas is unknown; (4) some gas reservoirs produce gas and water at the same time, and the water production is high [5,18–21]. Therefore, exploring the enrichment mechanism of deep shale gas is of great significance for understanding the exploration potential of deep shale gas resources, a shale gas enrichment model, and the sweet spot for the prediction of shale gas.

In this study, we used XRD, TOC, and other experimental methods to obtain the mineral composition, organic geochemistry, physical properties, and the gas- and water-bearing properties of the Longmaxi Formation shale in the Desheng–Yunjin syncline area. On this basis, the influence of the sedimentary environment, structural characteristics, and hydrodynamic conditions on shale gas enrichment in the study area were analyzed, and the deep shale gas-forming types were divided according to the main control factors. This study aims to reveal the enrichment law and forming type of deep shale gas and provide guidance for the exploration and development of deep shale gas.

2. Geological Setting

Sichuan Basin, located in the west of the paraplatform of the Yangtze plate, is one of the four major basins in China, with a total area of about 260,000 square kilometers (Figure 1a) [20–22]. The development of the Sichuan Basin is affected by the breakup of the peripheral blocks and the basement tectonic movement. The Nanhua period is an unstable rift, the Sinian period is a breakup basin, and the Cambrian period is a marginal extensional craton basin, which laid the basic framework of the Sichuan Basin [23,24]. Since then, the tectonic evolution of various regions in the Sichuan Basin has had obvious differences that can be divided into six structural units: the North Sichuan Basin, the Western Sichuan Basin, the Central Sichuan Basin, the Eastern Sichuan Basin, the Southwestern Sichuan Basin, and the Northwest Sichuan Basin (Figure 1a).

The Desheng–Yunjin syncline area is located in the southern Sichuan basin, crossing the Luzhou and Western Chongqing blocks. The study area can be divided into the Desheng syncline, the Baozang syncline, and the Yunjin syncline from west to east (Figure 1b). The target stratum of this study was the Silurian Longmaxi Formation shale. According to its sedimentary characteristics, Longmaxi Formation shale can be divided into the Long-1 member and the Long-2 member. The Long-1 member has graptolite development and high organic matter abundance, which is the main layer for deep shale gas exploration and development (Figure 1c).

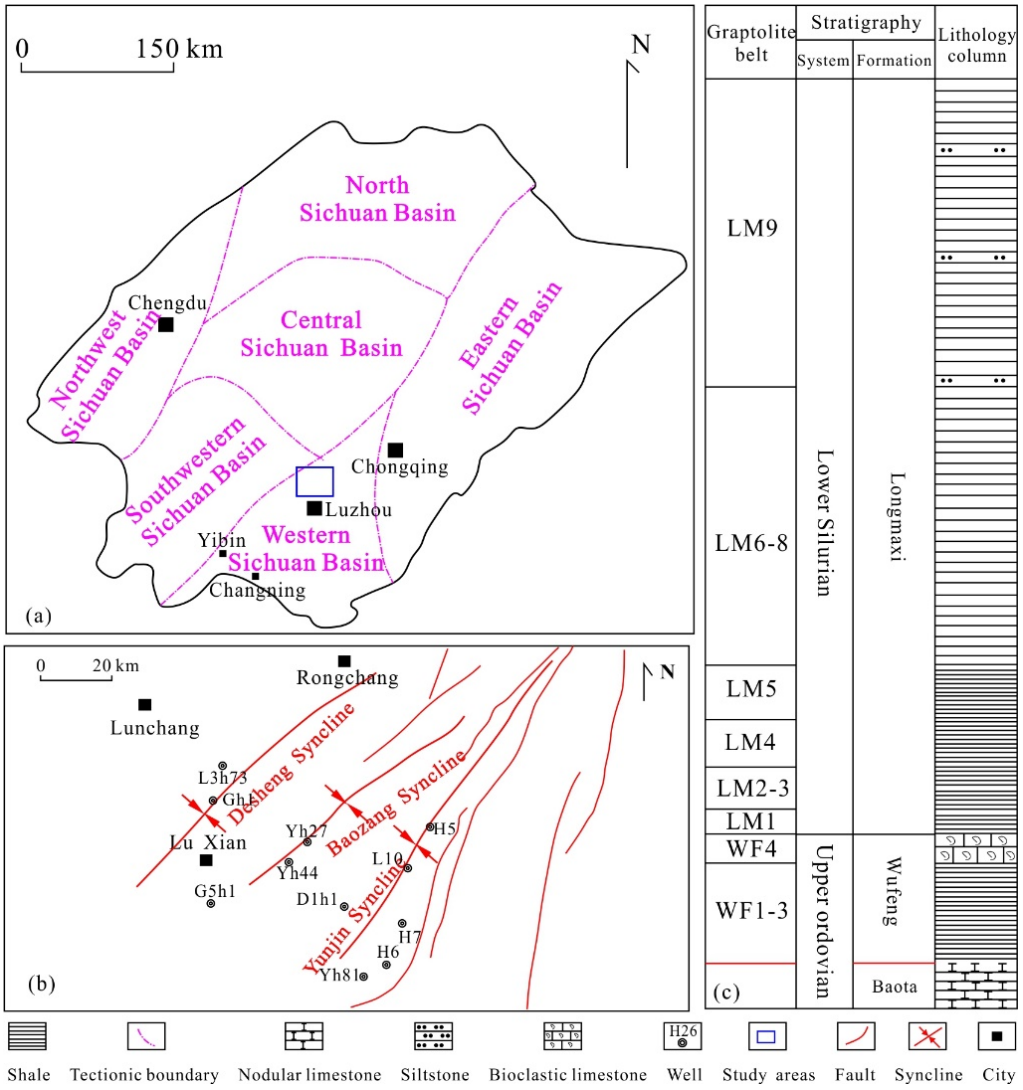

Figure 1. Geological overview of the Sichuan Basin and of the study area: (**a**) tectonic units of the Sichuan Basin (modified from [25]); (**b**) Location of the study area; (**c**) stratigraphic column of the lower Silurian and upper Ordovician.

3. Samples and Experiment

3.1. Samples

In this study, a total of 715 shale samples from 9 wells in the study area were collected, and all samples were tested for TOC. In addition, 713 samples were selected for a porosity test, 133 samples for a permeability test, 40 samples for an XRD test, 27 shale light sheets were prepared for observation of their organic macerals, and 23 samples for a bitumen reflectance test.

3.2. Experiment

The TOC test was conducted at the Analysis and Experiment Center of the Exploration and Development Research Institute of the PetroChina Southwest Oil and Gas Field Company. The instrument used was a carbon/sulfur analyzer. According to the Chinese National Standard GB/T 19145-2003, the shale sample was crushed to a powder with a particle size of less than 0.2 mm, an appropriate amount of sample was weighed, and excess hydrochloric acid was added to remove the inorganic carbon. Then, distilled water was added to dilute it to neutral, and the determination was carried out after drying. The temperature during the test was 17 °C, and the humidity was 59% RH.

The porosity of the shale samples was tested at the Analysis and Experiment Center of the Exploration and Development Research Institute of the PetroChina Southwest Oil and Gas Field Company. The testing instrument was a full-diameter plunger core porosity tester. According to the Chinese national standard GB/T 29172-2012, the porosity was tested three times at 23 °C and 60% RH.

The permeability was tested at the Sichuan Kelite Oil and Gas Technology Service Company Limited (Chengdu China). The instruments were a YCS-II briquette and a rock permeability tester. According to the Chinese National Standard GB/T 19145-2003, the permeability was measured using a non-steady state method (pressure pulse attenuation method). The test temperature was 17 °C, and the humidity was 55–60% RH.

XRD was carried out at Sichuan Kelite Oil and Gas Technology Service Company Limited (Chengdu China). The testing instrument used was an X'PertPowder X-ray diffractometer. According to the Chinese Industrial Standard SY/T 5163-2018, the shale sample was ground until the particle size was less than 40 μm. Samples (2 g) were weighed and the mineral composition and content were determined under 40 kV and 40 mA, with Cu radiation. The scanning speed was 2°/min and the scanning frequency was 0.02°.

The bitumen reflectance was measured at the Sichuan Kelite Oil and Gas Technology Service Company Limited (Chengdu China). with a polarizing microscope Axioscope A1 and spectrophotometer + MSP 400. All tests were conducted in accordance with the Chinese Industrial Standard SY/T 5124-2012.

In addition, the shale gas content and water saturation data used in this study are from the Exploration and Development Research Institute of the PetroChina Southwest Oil and Gas Field Company.

4. Results

4.1. Organic Petrology

The contents of organic macerals in the Longmaxi Formation shale in the study area were statistically analyzed, and the results are shown in Table 1. According to Table 1, the organic macerals of the Longmaxi Formation shale in the study area are mainly saprolite, with contents of 92~99% (average = 96%). The content of bitumen is low, with an average value of about 4%.

4.2. Mineralogy

Based on the XRD experimental results, the mineral composition of the Longmaxi Formation shale is shown in Table 2. According to Table 2, the mineral composition of the Longmaxi Formation shale in the study area is clay, quartz, rutile, dolomite, calcite, and pyrite, of which the clay is the highest (7~65%, with an average value of 36.95%), followed by quartz (21~80%, with an average value of 36.78%), feldspar (2~17%, with an average value of 7.53%), calcite (0~41%, with an average value of 7.48%), dolomite (0~30%, average of 6.83%), pyrite (0~9%, average of 3.88%), and rutile (0~2%, average of 0.58%).

The mineral composition of the Longmaxi Formation shale in the study area was analyzed using the ternary diagram of mineral composition. In the ternary diagram, the total content of quartz + feldspar + mica (QFM), calcite + dolomite + iron dolomite + siderite + magnesite (carbonate), and clay minerals is equal to 100% (Figure 2). The results show that the Longmaxi Formation shale in the study area can be divided into nine lithofacies types: silica-rich argillaceous mudstone, mixed argillaceous mudstone, argillaceous siliceous mudstone, mixed mudstone, clay-rich siliceous mudstone, mixed siliceous mudstone, mixed carbonate mudstone, carbonate-rich siliceous mudstone, and silica dominate mudstone. The main lithofacies types are silica-rich argillaceous mudstone, mixed mudstone, and argillaceous siliceous mudstone.

Table 1. Organic macerals and TI index of shale in the Longmaxi Formation in the study area.

Samples	Well	Maceral Content (%)					TI	Type
		Sapropelite	Bitumen	Exinite	Vitrinite	Inertinite		
L037-3-1	L3h73	98	2	0	0	0	96.5	I
L037-3-2	L3h73	99	1	0	0	0	98.25	I
L037-3-3	L3h73	94	6	0	0	0	89.5	I
L037-3-4	L3h73	95	5	0	0	0	91.25	I
L037-3-5	L3h73	95	5	0	0	0	91.25	I
L037-3-6	L3h73	96	4	0	0	0	93	I
Q2002004	Yh27	97	3	0	0	0	94.75	I
Q2002005	Yh27	98	2	0	0	0	96.5	I
Q2002006	Yh27	95	5	0	0	0	91.25	I
Q2002007	Yh27	95	5	0	0	0	91.25	I
Q2002008	Yh27	97	3	0	0	0	94.75	I
Q2002009	Yh27	93	7	0	0	0	87.75	I
Q2002010	Yh27	96	4	0	0	0	93	I
Q2002011	Yh27	96	4	0	0	0	93	I
Q2002012	Yh27	97	3	0	0	0	94.75	I
Q2002013	Yh27	94	6	0	0	0	89.5	I
Q2002014	Yh27	92	8	0	0	0	86	I
Q2002015	Yh27	97	3	0	0	0	94.75	I
Q2002016	Yh27	98	2	0	0	0	96.5	I
Q2030924	Yh44	97	3	0	0	0	94.75	I
Q2030933	Yh44	98	2	0	0	0	96.5	I
Q2030943	Yh44	96	4	0	0	0	93	I
Q2030953	Yh44	96	4	0	0	0	93	I
Q2030963	Yh44	97	3	0	0	0	94.75	I
Q2030973	Yh44	98	2	0	0	0	96.5	I
Q2030983	Yh44	95	5	0	0	0	91.25	I
Q2030993	Yh44	95	5	0	0	0	91.25	I

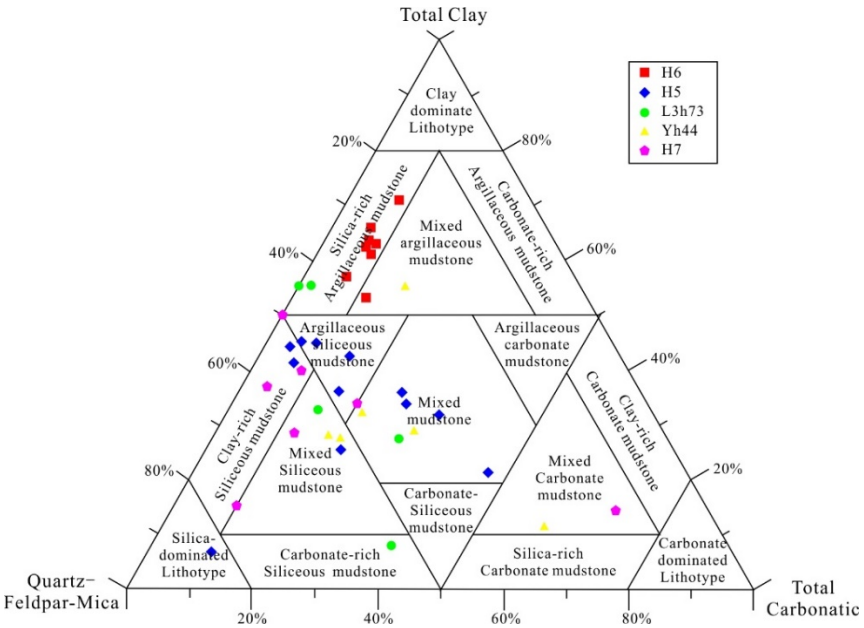

Figure 2. Shale facies division of the Longmaxi Formation in the study area (modified from [25]).

Table 2. Mineralogical characteristics of shale in the Longmaxi Formation.

Samples	Well	Depth (M)	Whole Rock Component (%)							Rock Component Content (%)			Brittleness Index
			Clay	Quartz	Feldspar	Calcite	Dolomite	Pyrite	Rutile	Total Clay	Carbonate	QFM	
H6-1	H6	4351.19	52	31	2	7	3	4	1	54.74	10.31	34.95	47
H6-2	H6	4352.2	57	27	1	6	3	4	2	60.64	9.47	29.89	41
H6-3	H6	4353.27	65	15	3	4	3	9	1	72.22	7.69	20.09	34
H6-4	H6	4354.24	51	26	6	5	3	9	0	56.04	8.79	35.16	49
H6-5	H6	4355.3	61	21	3	4	3	6	2	66.30	7.53	26.17	37
H6-6	H6	4356.19	61	21	5	6	3	4	0	63.54	9.18	27.27	39
H6-7	H6	4357.45	59	23	4	6	3	5	0	62.11	9.57	28.32	41
H6-8	H6	4358.38	58	22	3	6	3	7	1	63.04	9.89	27.07	41
H5-1	H5	4167.15	45	40	8	2	3	2	0	45.92	5.05	49.03	55
H5-2	H5	4168.1	41	36	7	7	7	2	0	41.84	14.89	43.27	59
H5-3	H5	4169.11	38	39	11	2	4	5	1	40.43	6.32	53.26	61
H5-4	H5	4170.04	32	33	8	6	17	3	1	33.33	28.40	38.27	67
H5-5	H5	4171.03	39	43	10	3	1	3	1	40.63	4.12	55.25	60
H5-6	H5	4172.09	42	40	9	4	1	4	0	43.75	5.26	50.99	58
H5-7	H5	4173.03	34	37	10	7	7	4	1	35.79	15.91	48.30	65
L037-3-1	L3h73	3701.42	55	33	10	2	0	0	0	55.00	2.00	43.00	45
L037-3-2	L3h73	3710.69	55	37	8	0	0	0	0	55.00	0.00	45.00	45
L037-3-3	L3h73	3720.4	27	42	10	12	6	3	0	27.84	19.78	52.38	73
L037-3-4	L3h73	3730.46	32	46	9	4	5	4	0	33.33	9.89	56.78	68
L037-3-5	L3h73	3740.43	31	43	8	5	8	5	0	32.63	14.94	52.43	69
L037-3-6	L3h73	3750.41	8	58	4	10	17	3	0	8.25	33.75	58.00	92
Q2030933	Yh44	4112.7	32	30	8	4	22	3	1	33.33	35.14	31.53	67
Q2030943	Yh44	4122.56	27	29	12	17	10	4	1	28.42	31.76	39.81	72
Q2030953	Yh44	4132.73	29	30	7	11	19	3	1	30.21	38.96	30.83	70
Q2030973	Yh44	4152.8	27	37	17	9	6	3	1	28.13	16.67	55.21	72
Q2030983	Yh44	4162.83	33	46	6	4	3	8	0	35.87	7.87	56.27	67
Q2030993	Yh44	4172.56	13	31	2	41	9	3	1	13.54	57.47	28.99	86
Q2032557	H7	4170.2	47	39	8	0	0	5	1	50.00	0.00	50.00	52
Q2032597	H7	4210.8	15	22	14	14	30	4	1	15.79	67.69	16.52	84
Q2032607	H7	4221.3	38	43	6	6	2	4	1	40.00	8.60	51.40	61
Q2032617	H7	4232.1	34	48	8	6	0	3	1	35.42	6.25	58.33	65

Table 2. *Cont.*

Samples	Well	Depth (M)	Whole Rock Component (%)							Rock Component Content (%)			Brittleness Index
			Clay	Quartz	Feldspar	Calcite	Dolomite	Pyrite	Rutile	Total Clay	Carbonate	QFM	
Q2032627	H7	4242.6	28	39	17	9	3	4	0	29.17	12.90	57.93	72
Q2032637	H7	4252.4	16	67	6	4	2	5	0	16.84	6.45	76.71	84
Q2032647	H7	4262.4	34	39	8	14	2	2	1	35.05	16.84	48.11	65
Q2030757	H5	4167.2	45	40	8	3	2	2	0	45.92	5.21	48.87	55
Q2030766	H5	4176.08	20	28	10	24	14	4	0	20.83	46.34	32.83	80
Q2030776	H5	4185.7	31	34	5	7	19	3	1	32.29	33.77	33.94	68
Q2030786	H5	4195.48	34	36	4	5	15	5	1	36.17	25.32	38.51	65
Q2030796	H5	4206.34	25	40	14	9	10	2	0	25.51	21.59	52.90	75
Q2030816	H5	4225.53	7	80	2	4	5	2	0	7.14	9.68	83.18	93

Previous studies have shown that the mineral composition and arrangement of rocks are of great significance to the removability of shale reservoirs [25–28]. It is generally believed that the higher the content of brittle minerals, the more favorable it is for later reservoir reconstruction. Previous scholars have often used the brittleness index to characterize the brittleness of shale, and brittle minerals mainly include carbonate, quartz, feldspar, and pyrite [26–29]. According to the brittleness index calculation formula in reference [25], the brittleness index of the Longmaxi Formation shale in the study area was calculated. The results show that the distribution span of the brittleness index of the Longmaxi Formation shale in the study area is large, 34–93, and the average value is 62. This indicates that the fracturing effect of the Longmaxi Formation shale in the later stage is complex.

4.3. Organic Geochemistry

4.3.1. Organic Matter Abundance

Organic matter abundance is the material basis for the hydrocarbon generation of source rocks and the most basic parameter for evaluating the quality of source rocks. It is commonly evaluated by parameters such as the total organic carbon (TOC) content and the hydrocarbon generation potential ($S_1 + S_2$) [2,30,31]. According to the statistics of 715 TOC data points of nine wells in the study area, the TOC of different wells (Figure 3a and Table 3) and a TOC frequency distribution value square diagram (Figure 3b) were prepared. The results show that the TOC of the Longmaxi Formation shale in the study area is mainly distributed in an interval of >2%. By comparing the distribution characteristics of the TOC in different wells, it was found that the TOC of the shale from different wells in the study area was more than 1%, and the TOC of some wells was more than 2%, which indicates that the Longmaxi Formation shale in the study area is mainly good source rock.

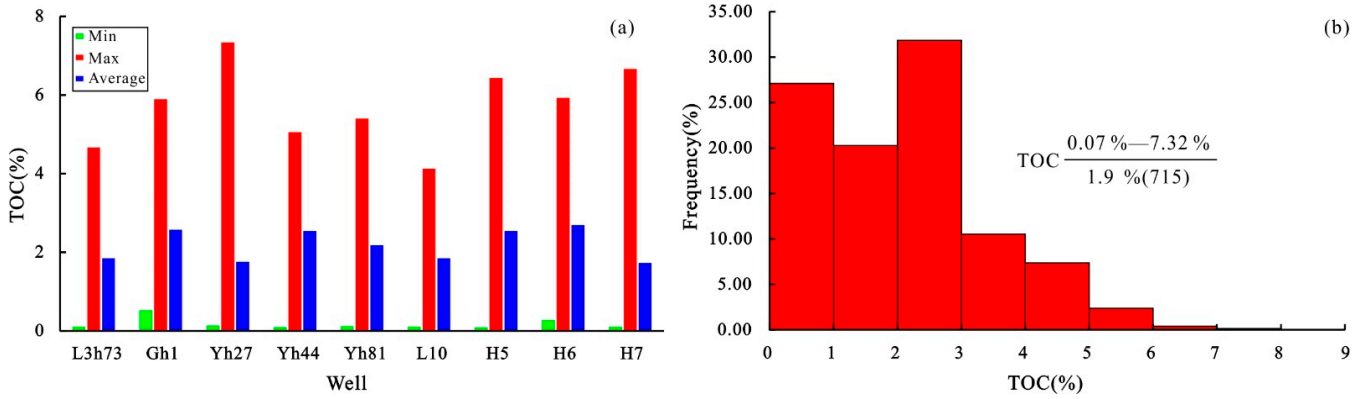

Figure 3. TOC frequency distribution histogram of the study area: (**a**) TOC distribution characteristics of different drilling wells; (**b**) TOC frequency distribution histogram.

Table 3. TOC statistics of different wells in the study area.

Well	TOC (%)			Number of Samples
	Min	Max	Average	
L3h73	0.09	4.65	1.83	56
Gh1	0.51	5.88	2.56	55
Yh27	0.12	7.32	1.74	125
Yh44	0.08	5.04	2.53	75
Yh81	0.1	5.39	2.16	92
L10	0.09	4.11	1.83	56
H5	0.07	6.42	2.53	65
H6	0.26	5.91	2.68	46
H7	0.09	6.65	1.71	111

4.3.2. Type of Organic Matter

The type of organic matter depends on the source of the original organic matter. Biochemical studies have shown that kerogen from different sources has different hydrocarbon generation potentials. Generally, kerogen from aquatic organisms has a stronger hydrocarbon generation capacity than that from terrestrial plants [32,33]. At present, there are many methods to determine the type of organic matter. In this study, the TI type index was used to determine the type of organic matter in the Longmaxi Formation shale in the study area. According to the classification of the TI type index [33], the organic matter type can be divided into four categories; 80–100 is type I, 40–80 is type II, 0–40 is type II-III, and <0 is type III.

The TI value of organic matter in the Longmaxi Formation shale in the study area was calculated according to the TI type index calculation formula in reference [32]. The results are shown in Table 1. According to Table 1, the shale macerals of the Longmaxi Formation in the study area are mainly saprolite, with contents of 92~99% and an average value of about 96%. The content of bitumen is low, with an average value of about 4%. The TI values range from 86 to 98.65, with an average value of 93.13. It is type I.

4.3.3. Maturity of Organic Matter

The maturity of the organic matter determines the amount of hydrocarbon generated during the geological history of the source rock, which is commonly characterized by vitrinite reflectance (Ro) and the maximum peak temperature of pyrolysis (Tmax) [2,34,35]. Based on the above discussion, the content of vitrinite in the Longmaxi Formation shale in the study area is extremely low. Therefore, the bitumen reflectance in the study area was measured. The results are shown in Table 4. According to Table 4, the bitumen reflectance (BRo) of the Longmaxi Formation shale in the study area is distributed between 3.11% and 3.52%, with an average reflectance of 3.28%.

Table 4. Statistical table of shale asphalt reflectance and vitrinite reflectance of the Longmaxi Formation shale in the study area.

Samples	Well	Bro (%)			Measuring Points	Ro (%)		
		Min	Max	Average		Min	Max	Average
Q2030933	Yh44	2.95	3.24	3.11	4	3.11	3.44	3.29
Q2030943	Yh44	2.89	3.27	3.12	5	3.05	3.47	3.30
Q2030953	Yh44	2.93	3.33	3.15	8	3.09	3.54	3.34
Q2030973	Yh44	3.02	3.34	3.19	10	3.19	3.55	3.38
Q2030983	Yh44	3.04	3.36	3.19	12	3.21	3.57	3.38
Q2030993	Yh44	3.09	3.43	3.25	8	3.27	3.65	3.45
Q2032557	H7	3.09	3.37	3.15	4	3.27	3.59	3.34
Q2032597	H7	3.11	3.55	3.31	15	3.29	3.79	3.52
Q2032607	H7	3.15	3.52	3.33	10	3.34	3.75	3.54
Q2032617	H7	3.14	3.49	3.34	12	3.33	3.72	3.55
Q2032627	H7	3.22	3.53	3.36	14	3.42	3.77	3.57
Q2032637	H7	3.24	3.54	3.35	11	3.44	3.78	3.56
Q2032647	H7	3.28	3.55	3.38	5	3.48	3.79	3.60
Q2030757	H5	2.99	3.34	3.19	10	3.16	3.55	3.38
Q2030766	H5	3.02	3.36	3.24	15	3.19	3.57	3.44
Q2030776	H5	2.97	3.38	3.25	10	3.14	3.60	3.45
Q2030786	H5	2.98	3.35	3.26	5	3.15	3.56	3.46
Q2030796	H5	3.03	3.38	3.28	4	3.20	3.60	3.48
Q2030816	H5	3.09	3.44	3.32	16	3.27	3.66	3.53
Q2016757	L3h73	3.04	3.43	3.31	10	3.21	3.65	3.52
Q2016767	L3h73	3.26	3.53	3.38	15	3.46	3.77	3.60
Q2016777	L3h73	3.35	3.58	3.43	12	3.56	3.82	3.65
Q2016787	L3h73	3.34	3.63	3.52	5	3.55	3.88	3.75

Previous studies have shown that there is a certain linear correlation between the BRo and the Ro, and when the Ro is in the range of 1.21% to 3.36%, the Ro = 1.125 and the BRo = 0.2062 [36]. This study used this formula to convert and calculate the Ro of the Longmaxi Formation shale in the study area. The results show that the Ro of the Longmaxi Formation shale in the study area is between 3.29% and 3.75%, and the average reflectance is 3.48%, which indicates that the Longmaxi Formation shale is in the over-mature stage.

4.4. Physical Properties of Shale

See Table 5 for the porosity and permeability test results of the plunger samples of the Longmaxi Formation in the study area. According to Table 5, the Longmaxi Formation shale is characterized by high porosity and low permeability. The porosity of the shale is 0.22~7.28% (average = 3.32%), and the permeability is 0.00104 $\times$ 10^{-3} μm^2~0.09805 $\times$ 10^{-3} μm^2, with an average of 0.01436 $\times$ 10^{-3} μm^2. This is an ultra-low permeability reservoir, which indicates that it is difficult to exploit the Longmaxi Formation shale. Hydraulic fracturing technology is required to increase the effective seepage channel and thus increase the production of shale gas.

Table 5. Statistical table of porosity and permeability of shale in the Longmaxi Formation in the study area.

Well	Porosity (%)				Permeability (10^{-3} μm^2)			
	Min	Max	Average	Number of Samples	Min	Max	Average	Number of Samples
L3h73	1.43	4.89	2.93	56	0.00104	0.09805	0.01245	51
Gh1	1.84	5.28	3.11	55				
Yh27	0.62	7.14	4.33	125	0.00313	0.07311	0.01554	82
Yh44	0.83	6.87	5.09	75				
L10	0.30	5.56	3.83	88				
H5	1.18	7.18	4.92	65				
H6	0.22	1.90	0.79	46				
H7	0.70	3.39	1.43	111				
Yh81	0.9	7.25	4.29	92				
Total	0.22	7.28	3.32	713	0.00104	0.09805	0.01436	133

4.5. Gas-Bearing Characteristics

According to the gas content of the Longmaxi Formation shale in different wells in the study area, the gas content contour map of the Longmaxi Formation shale in the study area is drawn, as shown in Figure 4. It can be seen in Figure 4 that the gas content of the Longmaxi Formation in the study area is mainly distributed in 4.5 m^3/t~8.1 m^3/t, with an average value of 5.9 m^3/t. In addition, the shale gas content of the Longmaxi Formation in the study area shows the characteristics of "high in the middle and low on both sides" from south to north.

4.6. Water Saturation

The water saturation levels of the Longmaxi Formation shale from different wells in the study area were determined, and the results are shown in Table 6. According to Table 6, the total water saturation of the Longmaxi Formation shale in the study area is high, distributed in 8.94~94.24%, with an average value of 48.68%.

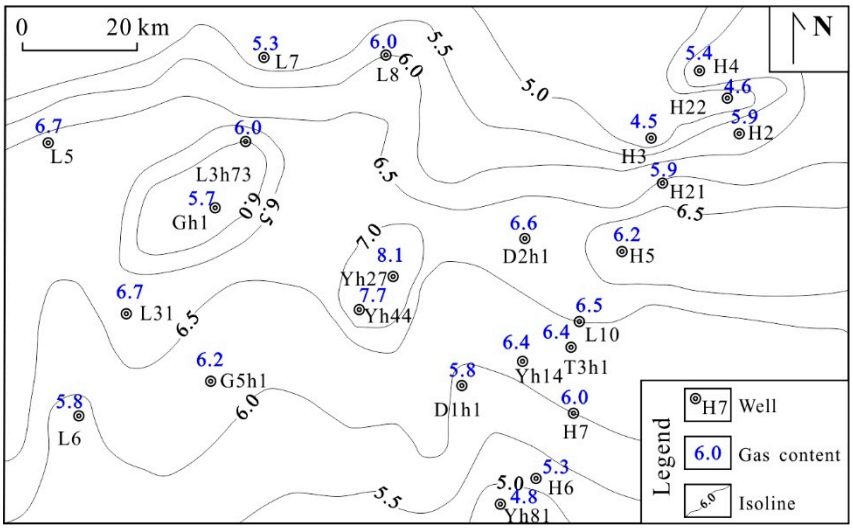

Figure 4. Contour map of shale gas content in the Longmaxi Formation in the study area.

Table 6. Water saturation of the Longmaxi Formation shale of different drilling wells in the study area.

Well	Water Saturation (%)			Number of Samples
	Min	Max	Average	
H5	16.17	85.42	41.26	65
H7	29.80	94.24	66.24	111
L3h73	22.26	88.63	67.47	55
Yh27	8.94	67.57	31.66	126
Yh81	40.75	83.15	61.81	92
Yh44	28.03	84.06	43.38	73
L10	11.84	77.47	51.63	92
Gh1	13.90	57.47	32.90	92
Total	8.94	94.24	48.68	706

5. Discussion

Previous studies have shown that the enrichment degree of shale gas is mainly related to sedimentary conditions, hydrocarbon generation evolution history, and later structural deformation degree [8–10]. However, recent scholars have found that the enrichment of shale gas is related to the water content in shale [13–16]. The types of water in shale are bound water, movable water, and capillary water. Bound water not only reduces the adsorption capacity of shale to methane gas, but it also occupies the storage space of methane, resulting in the reduction of its gas content [15–17]. In addition, capillary water and movable water in shale generate massive laminar flow or seepage under the action of the water head potential [15–17], which further affects the enrichment of shale gas. Based on this, this study took the Longmaxi Formation shale as an example to explore the factors controlling the enrichment of deep shale gas in the Desheng–Yunjin syncline from three aspects: sedimentary conditions, tectonic processes, and hydrogeological conditions.

5.1. Sedimentary Conditions

The influence of sedimentary conditions on shale gas accumulation is mainly manifested in two aspects: first, the reservoir development characteristics of the shale influence the shale gas accumulation; second, they control the lithology and distribution characteristics of shale roof and floor [17,18].

5.1.1. Control of Shale Development Characteristics on Shale Gas Enrichment

In order to accurately analyze the effects of shale characteristics on the enrichment and control of shale gas, the relationship between shale characteristics and gas content was determined (Figure 5). The results show that the gas content of shale in the Longmaxi Formation is weakly positively correlated with the TOC and porosity, weakly negatively correlated with the clay content, permeability, and water saturation, and has a trend of first increasing and then decreasing with the vitrinite reflectance, which is similar to the previous understanding. However, the correlation between the characteristics of shale in the Longmaxi Formation and the gas content is weak, which indicates that the characteristics of shale have a certain control effect on the gas content, but it is not the main control factor. The analysis shows that the gas content of shale in the Longmaxi Formation in the study area is greatly affected by other factors, such as tectonic activities.

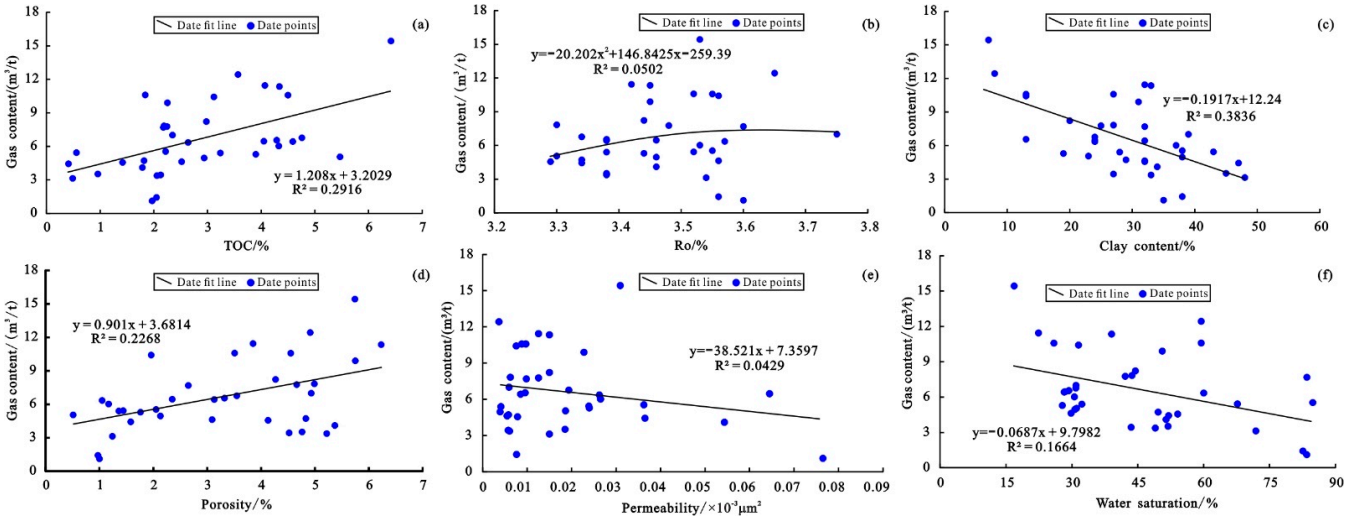

Figure 5. Relationship between shale development characteristics and gas content: (**a**) Relationship between TOC and gas content; (**b**) Relationship between Ro and gas content; (**c**) Relationship between TOC and clay content; (**d**) Relationship between porosity and gas content; (**e**) Relationship between permeability and gas content; (**f**) Relationship between water saturation and gas content.

5.1.2. Roof Sealing Property

The overlying strata of the Longmaxi Formation shale in the study area are the Shiniulan Formation, and the underlying strata are the Wufeng Formation and the Baota Formation. The Baota Formation and the Shiniulan Formation are thick massive nodular limestone. Since the drilling design was to stop drilling when the Baota Formation is 30 m, the thickness of the underlying strata of the Longmaxi Formation shale could not be calculated in this study.

The roof and floor, with good sealing properties, can reduce gas escape and migration, which is conducive to gas preservation [9,37–39]. Generally speaking, the denser and thicker the lithology of the roof, the more effective it is at preventing the escape of shale gas, which is conducive to the preservation of shale gas. According to the statistics of the thickness of the Shiniulan Formation—the overlying strata of the Longmaxi Formation—a correlation diagram between the thickness and the gas content was prepared, as shown in Figure 6. The results show that the correlation between the thickness of the Shiniulan Formation and the gas content of the overlying strata is poor, which indicates that the self-sealing property of the Longmaxi Formation shale is good, and the thickness of the roof has little effect on the enrichment of the Longmaxi Formation shale. This result is consistent with the characteristics of the overpressure reservoir of the Longmaxi Formation in the study area.

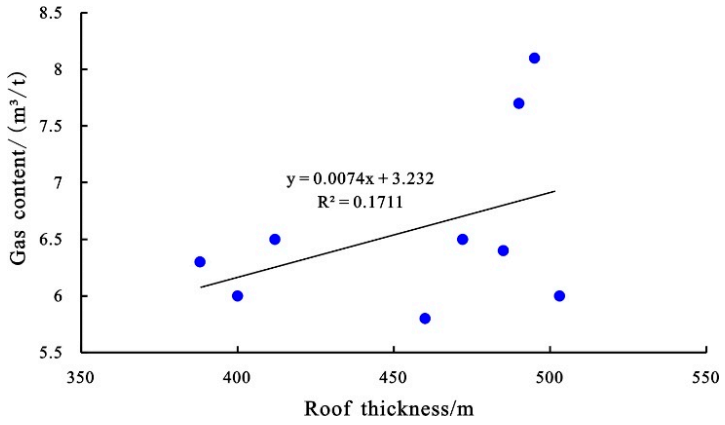

Figure 6. Relationship between overlying stratum thickness and gas content.

5.2. Tectonic Conditions

5.2.1. Control of Faults on Shale Gas Enrichment

The influence of faults on shale gas enrichment is mainly reflected in two aspects: one is the changing fracture degree and permeability of the shale reservoir; the other is that the faults themselves serve as channels for shale gas escape and migration [40,41]. According to the complexity of the regional geological structure, previous researchers have mainly discussed the influence of the fault structure on natural gas enrichment and productivity by dividing the structural zones [42–44]. According to the fault structure development characteristics of the Longmaxi Formation in the study area (Figure 7), the fault development degree in the north of the Desheng syncline and the Yunjin syncline is stronger than that in the south. The gas content in the north of the Desheng syncline and the Yunjin syncline is 5.3 m^3/t~6.0 m^3/t (average value is 5.75 m^3/t) and 4.5 m^3/t~5.9 m^3/t (average = 5.26 m^3/t), respectively, while the gas content in the south is 5.8 m^3/t~6.7 m^3/t (average value is 6.25 m^3/t) and 4.8 m^3/t~6.6 m^3/t (average value is 6.38 m^3/t), which is significantly higher than that in the north. In addition, the gas contents of wells H6, Yh81, and D1h1, close to the fault, are lower than 6 m^3/t, while the gas contents of wells Yh44 and Yh27, far from the fault, are higher than 7 m^3/t, which indicates that the fault development in the study area has a great impact on the shale gas enrichment, especially in the Yunjin syncline area.

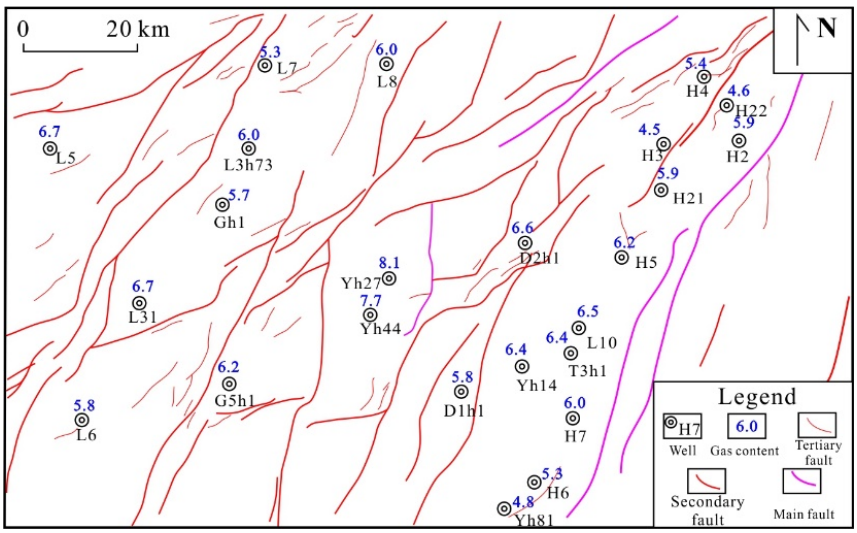

Figure 7. Fault development characteristics of the Longmaxi Formation in the study area.

5.2.2. Control of Fold on Shale Gas Enrichment

Due to tectonic activities, fold structures, such as the Desheng syncline, the Baozang syncline, and the Yunjin syncline developed in the study area. In combination with the structural bottom boundary map and fault development degree of the Longmaxi Formation in the study area, the drilling wells in the south of the study area were selected, and the projection method was used to prepare the relationship between the burial depth of the drilling profile and the gas content, as shown in Figure 8. According to Figure 8, the gas content of shale in the Longmaxi Formation of the Desheng syncline decreased with the increase in burial depth, that is, the gas content in the low structural parts is low, and the gas content in the high structural parts is high, which indicates that the shale gas enrichment in the Desheng syncline is greatly affected by the fold structure. At the Yunjin syncline, the gas content is positively correlated with the burial depth, which indicates that the shale gas enrichment in the south of the Yunjin syncline is less affected by the folds and is mainly controlled by the faults, while the Baozang syncline is not obvious.

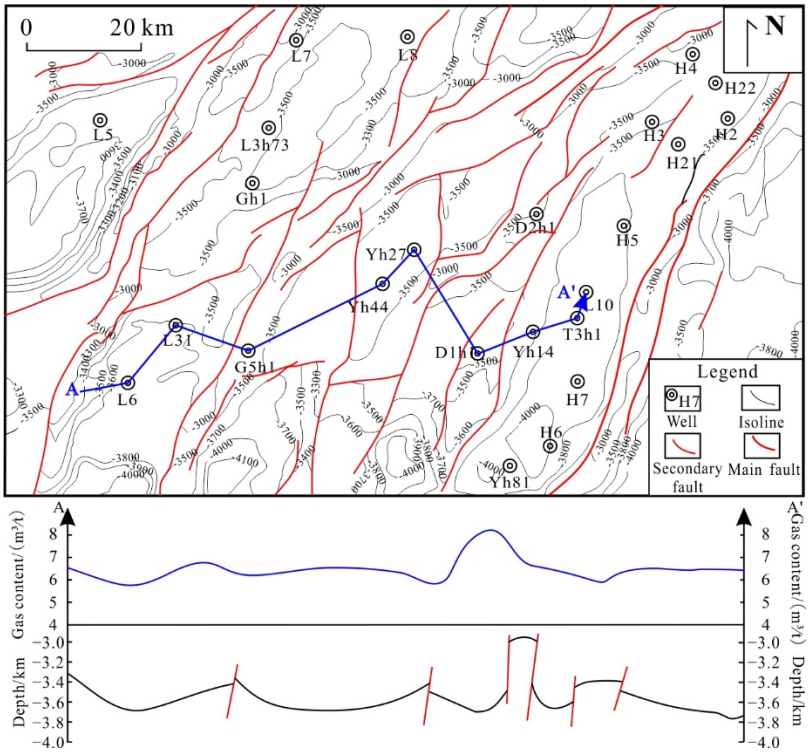

Figure 8. Comprehensive diagram of burial depth and gas content of the Longmaxi Formation drilling profile.

5.3. Hydrodynamic Conditions

Based on previous research results, the water in shale is bound water, capillary water, and movable water. Bound water is distributed in micropores, capillary water is distributed in pores of 10 nm–50 nm, and movable water is distributed in macropores [32,33]. At present, there are two viewpoints on the migration mode of water in shale. One is that the movable water moves in Darcy flow under the action of the head potential difference, while capillary water moves in pre-Darcy flow [33,45,46]. The other is that movable water and capillary water both move in Darcy flow under the action of the head potential, and the pre-Darcy flow is the experimental observation error [47,48]. Regardless of the migration mode, this indicates that there is a flow phenomenon of movable water in the shale.

Previous studies have shown that micropores, mesopores, and macropores are developed in the Longmaxi Formation shale in southern Sichuan, and the pore volume is mainly provided by mesopores and micropores, but the pore volume provided by macropores

accounts for about 24.6% of the pore volume of the whole rock [49,50], which indicates that there is a movement phenomenon of movable water in the Longmaxi Formation shale.

When there is a head potential difference in the study area, the movable water will flow under the action of the head potential difference. According to previous studies, the flow direction of the hydrodynamic force is from the high potential area to the low potential area. The groundwater in the high potential area is alternately active, and the water dissolution easily causes gas loss, while the low potential area has poor fluidity due to the pressure-bearing effect of water, which is conducive to oil and gas accumulation [51–53].

By calculating the converted water head potential of the Longmaxi Formation shale in different wells in the study area, the calculation formula of the converted water head potential is shown in document [51]. On this basis, three detention areas were divided, namely, the west of well L7, the surrounding area of well H3, and the areas of well Y3h1 and well Yh53 (Figure 9). Combined with the structural development and structural bottom boundary map of the study area, the gas content in the detention area and the runoff area were compared. The results show that the western part of well L7 in the detention area and the surrounding area of well H3 in the detention area are located in the northern part of the study area. The fault activity is developed and the gas content is lower than that in the runoff area, which indicates that the shale gas content in the area is weakly affected by the hydrodynamic force and mainly controlled by the fault development degree. Wells Y3h1 and Yh53 are located in the middle south of the study area, close to the core of the Baozang syncline, with relatively little structural development. The gas content in this area is less than that in the runoff area in the northwest, but higher than that in the southeast, which indicates that shale gas enrichment in this area is affected by hydrodynamic forces to a certain extent.

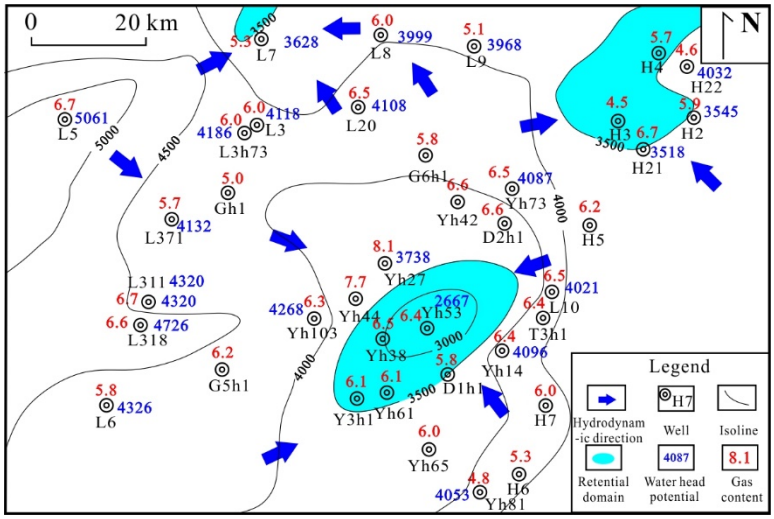

Figure 9. Shale gas content and hydrodynamic conditions of the Longmaxi Formation in the study area.

According to Figure 8, the northwest of wells Y3h1 and Yh53 is located at a high position of the structure, while the southeast is close to the elevation of wells Y3h1 and Yh53. This shows that the control effect of the hydrodynamic force on the shale gas in the northwest of wells Y3h1 and Yh53 is not obvious and mainly controlled by the fold structure, while the shale gas enrichment in the southeast of wells Y3h1 and Yh53 is mainly affected by the hydrodynamic force.

5.4. Forming Types of Deep Shale Gas Enrichment

Based on the above analysis, shale gas enrichment in the Desheng–Yunjin syncline area is mainly affected by the fault development degree, fold structure, and hydrodynamic

conditions. According to the drilling data, a reservoir-forming model map of the Longmaxi shale in the study area was prepared (Figure 10).

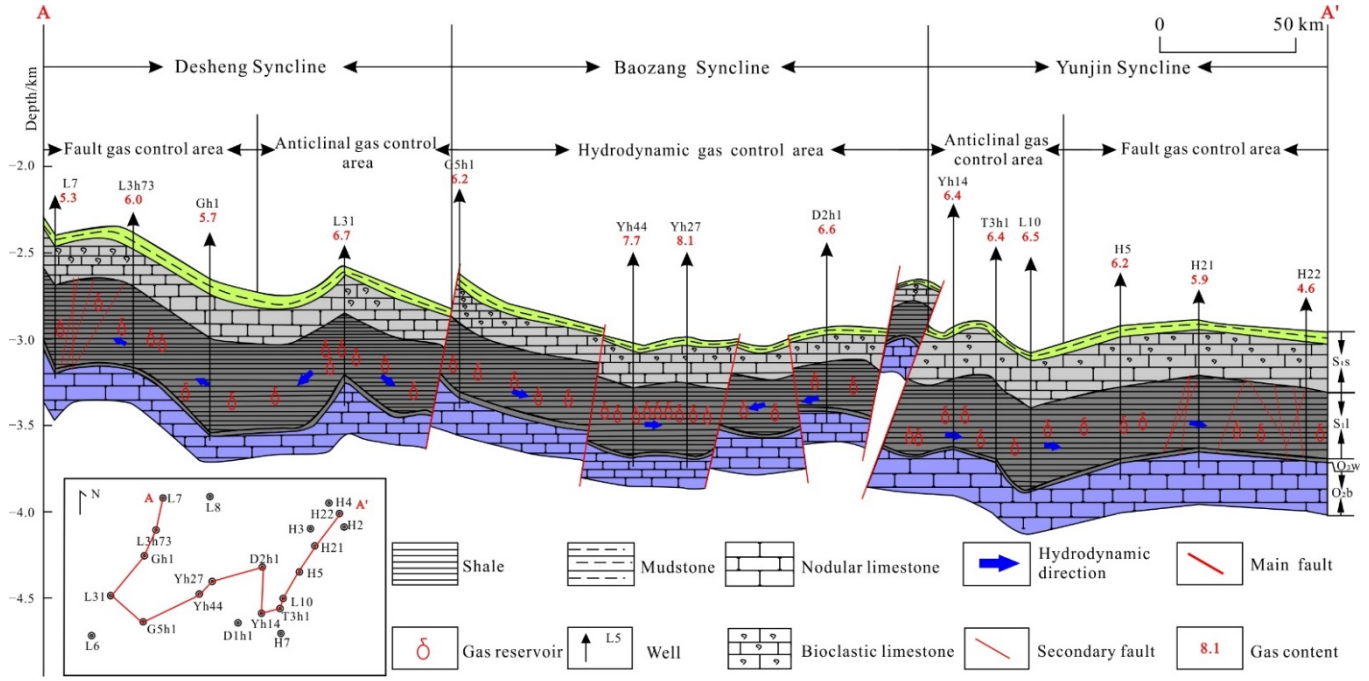

Figure 10. Shale gas enrichment pattern of the Longmaxi Formation in the Desheng–Yunjin Syncline area.

According to Figure 10, the northern part of the Desheng syncline is located at the high part of the structure, but the fault structure is developed in this area, and the shale gas escapes through the fault, resulting in the gas content of the high part being lower than that of the low part, indicating that this area is a fault-controlled shale gas accumulation type. In the south of the Desheng syncline, the fault structure is relatively less developed, and the gas content is generally characterized by low gas content in the low part and high gas content in the high structure part, indicating that the shale gas enrichment in this area is mainly controlled by the fold structure, which is the shale gas enrichment type controlled by the anticline. In the middle of the Baozang syncline, the gas content has a weak correlation with tectonic movement, but a good correlation with the hydrodynamic conditions. As a whole, the gas content in the detention area is higher than that in the runoff area, which indicates that the middle of the Baozang syncline is a type of shale gas enrichment controlled by hydrodynamic forces. The Yunjin syncline is similar to the Desheng syncline. The south is the shale gas accumulation type controlled by the anticline, and the north is the shale gas accumulation type controlled by the fault.

To sum up, the shale gas enrichment in the study area is mainly controlled by fault development, fold structure, and hydrodynamic conditions. Shale gas enrichment types can be divided into three types: fault-controlled gas, anticline-controlled gas, and hydrodynamic-controlled gas. Fault-controlled gas types are distributed in the north of the Desheng syncline and the north of the Yunjin syncline; anticline-controlled gas types are distributed in the south of the Desheng syncline and the south of Yunjin syncline; and hydrodynamic-controlled gas types are distributed in the middle of Baozang syncline.

6. Conclusions

Based on the characteristics of the organic petrology, organic geochemistry, mineralogy, petrophysical properties, and the gas- and water-bearing properties of the Longmaxi Formation shale in the Desheng–Yunjin syncline, this study analyzed the influence of the

sedimentary environment, structural characteristics, and hydrodynamic conditions on shale gas enrichment, and obtained the following conclusions:

(1) The Longmaxi Formation shale in the Desheng–Yunjin syncline area is a good hydrocarbon source rock as a whole. It is in the over-mature stage and has the characteristics of high porosity, low permeability, and high water saturation. The clay mineral and quartz content are high, and the brittleness indices are quite different. According to the mineral composition, nine lithofacies types can be found.

(2) The development characteristics of the shale and the sealing property of the roof of the Longmaxi Formation in the Desheng–Yunjin syncline have no obvious influence on the enrichment of the shale gas, but the tectonic activities and hydrodynamic conditions have obvious influence on the enrichment of the shale gas.

(3) The main controlling factors of the shale gas enrichment in different areas in the Desheng–Yunjin Syncline area are different. According to the main controlling factors, there are three types of gas accumulation: fault-controlled gas, anticline-controlled gas, and hydrodynamic-controlled gas. The fault-controlled gas type is distributed in the north of the Desheng syncline and the north of the Yunjin syncline; the anticline-controlled gas type is distributed in the south of the Desheng syncline and the south of the Yunjin syncline; and the hydrodynamic-controlled gas type is distributed in the middle of the Baozang syncline.

Author Contributions: Conceptualization, X.S. and W.W.; methodology, Q.W.; validation, X.S., W.W. and H.M.; formal analysis, K.Z.; investigation, W.W., Q.W. and K.Z.; resources, X.S., W.W., Q.W. and Z.J.; data curation, X.S. and H.M.; writing—original draft preparation, H.M., Z.J. and X.S.; writing—review and editing, Z.J. and H.M.; visualization, W.W. and Z.J.; supervision, X.S., W.W., Q.W. and Z.J.; project administration, X.S., W.W., Q.W. and Z.J.; funding acquisition, X.S., W.W., Q.W. and Z.J. All authors have read and agreed to the published version of the manuscript.

Funding: This study was supported by the National Major Science and Technology Project of China (grant nos. 2017ZX05035-02 and 2016ZX05034-001-05) and the Innovative Research Group Project of the National Natural Science Foundation of China (grant nos. 41872135 and 42072151). We thank the Analysis and Experiment Center of the Exploration and Development Research Institute of the PetroChina Southwest Oil and Gas Field Company, the Sichuan Kelite Oil and Gas Technology Service Co., Ltd., and the China University of Petroleum, Beijing, for providing the testing samples and test equipment, as well as our colleagues' useful suggestions.

Conflicts of Interest: The authors declare no competing financial interest.

References

1. Gang, Z.W.; Wang, Q.Y.; Luo, J.Q. Oil and gas resource potential of the lower members of E-h3 in the lower Tertiary of the Biyang Depression, China. *Petrol. Sci.* **2012**, *9*, 18–24. [CrossRef]
2. Miao, H.; Wang, Y.B.; Zhao, S.H.; Guo, J.Y.; Ni, X.M.; Gong, X.; Zhang, Y.J.; Li, J.H. Geochemistry and organic petrology of middle permian source rocks in taibei sag, Turpan-Hami Basin, China: Implication for organic matter enrichment. *ACS Omega* **2021**, *6*, 31578–31594. [CrossRef] [PubMed]
3. Guo, T.L. Key geological issues and main controls on accumulation and enrichment of Chinese shale gas. *Pet. Exp. Dev.* **2016**, *43*, 349–359. [CrossRef]
4. Nie, H.K.; Li, P.; Dang, W.; Ding, J.H.; Sun, C.X.; Liu, M.; Wang, J.; Du, W.; Zhang, P.X.; Li, D.H.; et al. Enrichment characteristics and research directions of deep shale gas: A case study of the Ordovician Wufeng-Silurian Longmaxi shale in the Sichuan Basin and its surrounding areas, China. *Pet. Exp. Dev.* **2022**, *49*, 648–659.
5. Wan, Y.; Tang, S.H.; Pan, Z.J. Evaluation of the shale gas potential of the lower Silurian Longmaxi Formation in northwest Hunan Province, China. *Mar. Pet. Geol.* **2018**, *79*, 159–175. [CrossRef]
6. Jiang, Z.X.; Song, Y.; Tang, X.L.; Li, Z.; Wang, X.M.; Wang, G.Z.; Xue, Z.X.; Zhang, K.; Chang, J.Q.; Qiu, H.Y. Controlling factors of marine shale gas differential enrichment in southern China. *Pet. Exp. Dev.* **2020**, *47*, 617–628. [CrossRef]
7. Wang, E.Z.; Guo, T.L.; Li, M.W.; Xiong, L.; Dong, X.X.; Zhang, N.X.; Wang, T. Depositional environment variation and organic matter accumulation mechanism of marine-continental transitional shale in the upper permian longtan formation, Sichuan Basin, SW China. *ACS Earth Space Chem.* **2022**, *6*, 2472–3452. [CrossRef]
8. Hao, F.; Zou, H.Y. Cause of shale gas geochemical anomalies and mechanisms for gas enrichment and depletion in high-maturity shales. *Mar. Pet. Geol.* **2013**, *44*, 1–12. [CrossRef]

9. Yasin, Q.; Baklouti, S.; Khalid, P.; Ali, S.H.; Boateng, C.D.; Du, Q.Z. Evaluation of shale gas reservoirs in complex structural enclosures: A case study from Patala Formation in the Kohat-Potwar Plateau, Pakistan. *J. Pet. Sci. Eng.* **2021**, *198*, 108225. [CrossRef]
10. Shi, Y.G.; Tang, X.L.; Wu, W.; Jiang, Z.X.; Xiang, S.J.; Wang, M.; Zhou, Y.R.; Xiao, Y.P. Control of complex structural deformation and fractures on shale gas enrichment in southern Sichuan Basin, China. *Energy Fuels* **2022**, *36*, 6229–6242. [CrossRef]
11. Dang, W.; Zhang, J.C.; Nie, H.K.; Wang, F.Q.; Tang, X.; Wu, N.; Chen, Q.; Wei, X.L.; Wang, R.J. Isotherms, thermodynamics and kinetics of methane-shale adsorption pair under supercritical condition: Implications for understanding the nature of shale gas adsorption process. *Chem. Eng. J.* **2020**, *383*, 123191. [CrossRef]
12. Dang, W.; Zhang, J.C.; Tang, X.; Wei, X.L.; Li, Z.M.; Wang, C.H.; Chen, Q.; Liu, C. Investigation of gas content of organic-rich shale: A case study from Lower Permian shale in southern North China Basin, central China. *Geosci. Front.* **2018**, *9*, 559–575. [CrossRef]
13. Li, X.Y.; Chen, S.B.; Wang, Y.W.; Zhang, Y.K.; Wang, Y.; Wu, J.F.; Zhang, J.J.; Khan, J. Influence of pore structure particularity and pore water on the occurrence of deep shale gas: Wufeng-Longmaxi Formation, Luzhou Block, Sichuan Basin. *Nat. Res. Res.* **2022**, *31*, 1403–1423. [CrossRef]
14. Li, Q.; Lu, H.; Li, J.S.; Wu, S.H.; Wu, Y.; Wen, L.; He, Y.; Qi, F.Q. Characteristics and Formation mechanism of the tight tuff reservoirs of the Upper Triassic Chang 7 member in the southern Ordos Basin, China. *Mar. Pet. Geol.* **2022**, *139*, 105625. [CrossRef]
15. Li, J.Q.; Lu, S.F.; Zhang, P.F.; Li, W.B.; Jing, T.Y.; Feng, W.J. Quantitative characterization and microscopic occurrence mechanism of pore water in shale matrix. *Acta Pet. Sin.* **2020**, *41*, 979–990. (In Chinese with English Abstract)
16. Yang, S.; Yu, Q. Experimental investigation on the movability of water in shale nanopores: A case study of Carboniferous shale from the Qaidam Basin, China. *Water Resour. Res.* **2020**, *56*, e2019WR026973. [CrossRef]
17. Yan, D.Y.; Huang, W.H.; Lu, X.X.; Yin, X.D.; Shi, Y.L. Contrast of reservoir-forming conditions of marine-continental transitional shale gas in different sedimentary environments in the Lower Yangtze area of China. *J. China Coal Soc.* **2016**, *41*, 1778–1787. (In Chinese with English Abstract)
18. Zhang, H.J.; Jiang, Y.Q.; Zhou, K.M.; Fu, Y.H.; Zhong, Z.Z.; Zhang, X.M.; Qi, L.; Wang, Z.L.; Jiang, Z.Z. Connectivity of pores in shale reservoirs and its implications for the development of shale gas: A case study of the Lower Silurian Longmaxi Formation in the southern Sichuan Basin. *Nat. Gas Ind.* **2019**, *39*, 22–31. (In Chinese with English Abstract) [CrossRef]
19. Nie, H.K.; Jin, Z.J. Source rock and cap rock controls on the Upper Ordovician Wufeng Formation-Lower Silurian Longmaxi Formation shale gas accumulation in the Sichuan Basin and its Peripheral Areas. *Acta Geol. Sin.-Engl. Ed.* **2016**, *90*, 1059–1060.
20. Shi, X.W.; Kang, S.J.; Luo, C.; Wu, W.; Zhao, S.X.; Zhu, D.; Zhang, H.X.; Yang, Y.; Xiao, Z.L.; Li, Y. Shale gas exploration potential and reservoir conditions of the Longmaxi Formation in the Changning area, Sichuan Basin, SW China: Evidence from mud gas isotope logging. *J. Asian Ear. Sci.* **2022**, *233*, 105239. [CrossRef]
21. Fan, C.H.; Li, H.; Qin, Q.R.; He, S.; Zhong, C. Geological conditions and exploration potential of shale gas reservoir in Wufeng and Longmaxi Formation of southeastern Sichuan Basin, China. *J. Petrol. Sci. Eng.* **2020**, *191*, 107138. [CrossRef]
22. Li, Z.Q.; Ying, D.L.; Li, H.K.; Yang, G.; Zeng, Q.; Guo, X.Y.; Chen, X. Evolution of the western Sichuan basin and its superimposed characteristics, China. *Acta Pet. Sin.* **2011**, *27*, 2362–2370.
23. Miao, Z.S.; Pei, Y.W.; Su, N.; Sheng, S.Z.; Feng, B.; Jiang, H.; Liang, H.; Hong, H.T. Spatial and temporal evolution of the Sinian and its implications on petroleum exploration in the Sichuan Basin, China. *J Pet. Sci. Eng.* **2022**, *210*, 110036. [CrossRef]
24. Liu, S.G.; Yang, Y.; Deng, B.; Zhong, Y.; Wen, L.; Sun, W.; Li, Z.W.; Jansa, L.; Li, J.X.; Song, J.M.; et al. Tectonic evolution of the Sichuan Basin, Southwest China. *Ear. Sci. Rew.* **2021**, *213*, 103470. [CrossRef]
25. Li, W.; Yu, H.Q.; Deng, H.B. Stratigraphic division and correlation and sedimentary characteristics of the Cambrian in central-southern Sichuan Basin. *Pet. Exp. Dev.* **2012**, *39*, 725–735. [CrossRef]
26. Glaser, K.S.; Miller, C.K.; Johnson, G.M.; Kleinberg, R.L.; Pennington, W.D. Seeking the sweet spot: Reservoir and completion quality in organic shales. *Oilfield Rev.* **2014**, *25*, 16–29.
27. Kumar, S.; Das, S.; Bastia, R.; Ojha, K. Mineralogical and morphological characterization of Older Cambay Shale from North Cambay Basin, India: Implication for shale oil/gas development. *Mar. Pet. Geol.* **2018**, *97*, 339–354. [CrossRef]
28. Rimstidt, J.D.; Chermak, J.A.; Schreiber, M.E. Processes that control mineral and element abundances in shales. *Earth Sci. Rev.* **2017**, *171*, 383–399. [CrossRef]
29. Zhao, S.H.; Wang, Y.B.; Li, Y.; Li, H.H.; Xu, Z.H.; Gong, X. Geochemistry and mineralogy of Lower Paleozoic Heituao Shale from Tadong Low Uplift of Tarim Basin, China: Implication for Shale Gas development. *Minerals* **2021**, *11*, 635. [CrossRef]
30. Prommer, H.; Davis, G.B.; Barry, D.A. Geochemical changes during biodegradation of petroleum hydrocarbons: Field investigations and biogeochemical modelling. *Org. Chem.* **1999**, *30*, 423–435. [CrossRef]
31. Makeen, Y.M.; Abdullah, W.H.; Hakimi, M.H.; Mustapha, K.A. Source rock characteristics of the Lower Cretaceous Abu Gabra Formation in the Muglad Basin, Sudan, and its relevance to oil generation studies. *Mar. Pet. Geol.* **2015**, *59*, 505–516. [CrossRef]
32. Cao, Q.Y. Identification of microcomponents and types of kerogen under transmitted light. *Pet. Exp. Dev.* **1985**, *12*, 14–23. (In Chinese with English Abstract)
33. Shen, J.N.; Yang, J.Y.; Zhou, F.; Zhang, J.; Yang, G.N.; Qiu, Y.P.; Sun, Y. Study of kerogen type index thorough the calculation of organic elements. *J. Northeast Pet. Univ.* **2013**, *5*, 24–31. (In Chinese with English Abstract)
34. Jarvie, D.M.; Claxton, B.L.; Henk, F.; Breyer, J.T. Oil and shale gas from the Barnett Shale, Ft. In *Worth Basin, Texas; AAPG Annual Meeting Program*; AAPG: Denver, CO, USA, 2001.
35. Laubach, S.E.; Olson, J.E.; Gross, M.R. Mechanical and fracture stratigraphy. *AAPG Bull.* **2009**, *93*, 1413–1426. [CrossRef]

36. Wang, Y.; Qiu, N.S.; Ma, Z.L.; Ning, C.X.; Zheng, J.L.; Zhou, Y.Y.; Fang, G.J.; Rui, X.Q.; Rao, D. Evaluation of equivalent relationship between vitrinite reflectance and solid bitumen reflectance. *J. China Univ. Min. Technol.* **2020**, *49*, 563–575. (In Chinese with English Abstract)
37. Xu, L.L.; Huang, S.P.; Liu, Z.X.; Zhang, Y.L.; Wen, Y.R.; Zhou, X.H.; Chen, W.; Ren, Z.J.; Wen, J.H. Paleoenvironment Evolutionary Characteristics of Niutitang Shale in Western Hubei, Middle Yangtze, China. *ACS Omega* **2022**, *7*, 24365–24383. [CrossRef]
38. Poprawski, Y.; Basile, C.; Cumberpatch, Z.; Eude, A. Mass transport deposits in deep-water minibasins: Outcropping examples from the minibasins adjacent to the Bakio salt wall (Basque Country, Northern Spain). *Mar. Pet. Geol.* **2021**, *132*, 105194. [CrossRef]
39. Cui, Z.; Yang, W.; Wang, Q.Y.; Zuo, R.S.; Cai, J.F.; Cui, Z.J.; Xu, L.; Li, L.; Gu, X.M. Sealing property of roof and floor of Wufeng Formation-Longmaxi Formation and its influence on shale gas differential enrichment in Sichuan Basin and its surrounding areas. *Mar. Orig. Pet. Geol.* **2020**, *25*, 243–252.
40. Miao, H.; Wang, Y.B.; He, C.; Li, J.H.; Zhang, W.; Zhang, Y.J.; Gong, X. Fault development characteristics and reservoir control in Chengbei fault step zone, Bohai Bay Basin. *Lithol. Reserv.* **2022**, *34*, 105–115. (In Chinese with English Abstract)
41. Wang, H.M.; Fan, C.H.; Fang, Y.; Zhao, S.X.; Shi, X.C.; Liu, J.F.; Yang, H.F.; Hu, J.; Lian, C.B. Structural analysis and evolution model of the Longmaxi Formation in the Yanjin-Junlian Area of the southern Sichuan Basin, China. *Front. Earth Sci.* **2022**, *10*, 884971. [CrossRef]
42. Hu, X.Q.; Liu, H.; Tan, X.C.; Dan, Y.; He, H.; Xiao, C.J.; Li, R.X. Characteristics of Karst Formations and their significance for shale gas exploration. *Front. Earth Sci.* **2022**, *10*, 907685. [CrossRef]
43. Wang, F.T.; Guo, S.B. Upper paleozoic transitional shale gas enrichment factors: A Case study of typical areas in China. *Minerals* **2020**, *10*, 194. [CrossRef]
44. Fan, C.H.; Xie, H.B.; Li, H.; Zhao, S.X.; Shi, X.C.; Liu, J.F.; Meng, L.F.; Hu, J.; Lian, C.B. Complicated fault characterization and its influence on shale gas preservation in the southern margin of the Sichuan Basin, China. *Lithosphere* **2022**, *2022*, 8035106. [CrossRef]
45. Wang, L.; Yu, Q. The effect ofmoisture on the methane adsorption capacity ofshales: A study case in the eastern Qaidam Basin in China. *J. Hydrol.* **2016**, *542*, 487–505. [CrossRef]
46. Diwu, P.; Liu, T.; You, Z.; Jiang, B.; Zhou, J. Effect of low velocity non-Darcy flow on pressure response in shale and tight oil reservoirs. *Fuel* **2018**, *216*, 398–406. [CrossRef]
47. Olsen, H.W. Darcy's law in saturated kaolinite. *Water Resour. Res.* **1966**, *2*, 287–295. [CrossRef]
48. Wang, X.; Sheng, J.J. Effect oflow-velocity non-Darcy flow on well production performance in shale and tight oil reservoirs. *Fuel* **2017**, *190*, 41–46. [CrossRef]
49. Jiang, Z.X.; Li, X.; Wang, X.M.; Wang, G.Z.; Qiu, H.Y.; Zhu, D.Y.; Jiang, H.Y. Characteristic differences and controlling factors of pores in typical South China shale. *Oil Gas Geol.* **2021**, *42*, 41–53. (In Chinese with English Abstract)
50. Jiang, Z.X.; Tang, X.L.; Li, Z.; Huang, H.X.; Yang, P.P.; Yang, X.; Li, W.B.; Hao, J. The whole-aperture pore structure characteristics and its effect on gas content of the Longmaxi Formation shale in the southeastern Sichuan basin. *Earth Sci. Front.* **2016**, *23*, 126–134. (In Chinese with English Abstract)
51. Song, Y.; Liu, S.B.; Ma, X.Z.; Jiang, L.; Hong, F. Favorable depth distribution of coalbed methane enrichment and high yield zone in slope areas. *Acta Geol. Sin.-Engl. Ed.* **2017**, *91*, 371–372. [CrossRef]
52. Revil, A.; Leroy, P. Constitutive equations for ionic transport in porous shales. *J. Geophys. Res.* **2004**, *109*, B03208. [CrossRef]
53. Tian, W.G.; Tang, D.Z.; Sun, B.; Zhao, S.P.; Wen, J. hydrodynamic conditions and their controls of gas in coal-bearing strata in Eastern Edge of the Ordos Basin. *Geol. J. China Univ.* **2012**, *18*, 433–437. (In Chinese with English Abstract) [CrossRef]